J Mater Sci: Mater Med (2008) 19:1529–1535
DOI 10.1007/s10856-008-3382-9

Nanomechanical characterization of red blood cells using optical tweezers

Chuan Li · K. K. Liu

Received: 4 October 2007 / Accepted: 4 January 2008 / Published online: 24 January 2008

Abstract Deformation behaviours of red blood cells (RBCs) have been studied by applying stretching forces via optical tweezers. Combined with finite-element analyses (FEA), the RBCs' mechanical properties are determined quantitatively based on a best fitting between the experimental deformed geometries and the simulated counterparts. Experimentally, a silica beads attached erythrocyte is optical-mechanically stretched to different lengths. On the theoretical front, a large deformation model with Mooney-Rivlin constitutive equations has been simulated by using FEA to predict the cell deformation geometries. The numerically simulated transverse and longitudinal strains which are in a good agreement with the experimental measurements facilitate the determination of elastic constants of the cells.

1 Introduction

It is well recognized that the mechanical properties of erythrocyte are crucial for maintaining cell functions and their changes are associated with many important physiological/pathological processes. For example, sickle erythrocytes have less deformability and obvious fragility [1], while malaria-infected red blood cells (RBCs) have notable alternation in the mechanical properties of cell membrane [2]. The changes of the cell mechanical properties can therefore be regarded as a prelude to the pathogenesis of certain diseases [3]. Moreover, RBC used as a physiological carrier for delivering proteins and molecules as therapeutics has recently been regarded as a fascinating attempt for the next generation of drug delivery [4]. The RBC mechanical property which may be modified by loading with pharmacological substances is considered as a key parameter to govern the delivery behaviours throughout the human body. Hence, mechanical characterization of erythrocyte is of paramount importance in the advancement of the erythrocyte-based therapeutic delivery.

Optical tweezers have emerged as a useful tool for manipulating single biological cells and performing sophisticated biomechanical characterizations, such as estimation of the cell membrane elasticity [5]. The unique advantages of using optical tweezers for these characterizations include non-contact force for cell manipulation, force resolution as accurate as sub-nano-Newton and amiability to liquid medium environments [6]. The major concern for using optical tweezers is the laser heating which often increase cell temperatures and has effect on cell viability and however such heating can be eliminated by using microbeads attached on the cells as handlers for the focused laser beams [6].

In this study, both experimental and numerical studies have been carried out to determine the deformation and mechanical properties of single erythrocytes. For the experimental part, RBCs were first chemically swollen and attached by silica beads then stretched by optical tweezers. The deformation of cells can be measured from their digital images and characterized by the longitudinal and transverse strains. On the numerical front, finite-element

C. Li
School of Mechanical and Aerospace Engineering, Nanyang Technological University, 50 Nanyang Ave., Singapore, Singapore 639798
e-mail: mcli@ntu.edu.sg

K. K. Liu (✉)
Institute of Science and Technology in Medicine, Keele University, Thornburrow Drive, Stoke-on-Trent ST4 7QB, UK
e-mail: i.k.liu@keele.ac.uk

analyses (FEA) have been applied to simulate the RBC deformation with the Mooney–Rivilin material model. A comparison between the experimental and numerical data was conducted to determine appropriate range of material constants proposed in the Mooney–Rivilin model. The study has demonstrated both capability and potential of optical tweezers in combination with FEA in quantitative determination of the mechanical behaviours of biological cells.

2 Materials and methods

2.1 Preparations of the RBCs

Fresh blood of white rats was extracted and kept in acid citrate dextrose (Sigma C3821, an anticoagulant) at 4°C. Before the each experiment performed, an aliquot of blood sample was diluted in the phosphate-buffered saline (PBS, Sigma P4417) and then rinsed and fractionated through a centrifuge three times. In parallel, silica microbeads (Fishers, IN, US) were washed in deionized water and then centrifuged for several times. Through the routine washing process, contaminant on the beads was removed spontaneous and non-specific adhesion between the RBCs and microbeads can therefore be ensured in the later cell-bead attachment process. The diameters of the beads were measured between 2 and 3 μm.

The washed microbeads and RBCs were diluted again by the PBS to the concentration of 2×10^5 and 1×10^5/μl, respectively. The bead-cell concentration ratio of 2:1 is to encourage every two beads adhering on one erythrocyte. After diluting, 20 μl of each suspension were mixed together in a vial. The mixed suspension was incubated at 4°C for 1 h to foster the adhesion between the RBCs and microbeads [7]. Once the adhesion was ensured via an optical microscopic investigation, the mixed suspension was further diluted to about 1×10^3 cells/μl in a hypotonic buffer (10 mM potassium phosphate, 75 mM NaCl at pH 7.4, i.e., 155 mOsm/kg), with a small amount (ca. 1 mg/ml) of bovine serum albumin (Sigma A4503) added to prevent RBCs from sticking on the glass plate [8]. This suspension was kept at 37°C for about 10–20 min before the experiment of laser trapping started for allowing RBCs to be osmotically inflated into a nearly spherical shape.

2.2 Optical laser tweezers

A commercial optical tweezers system (Module 1064/1500 from Cell Robotic, Inc, USA) is used in the present experimental work. A laser source (Nd:YAG) which was pumped by a 1.5 W diode generated a light with a wavelength of 1,064 nm [9]. The laser light was then reflected through dichroic mirrors and focused through an inverted microscope (DMIL, LEICA, Germany) before it trapped the microbeads. The trapping force is then aimed to drag the beads/cells by moving it through the buffer solution inside a chamber placed on the motorized XY table of the optical tweezers system.

2.3 Measurements

The deformation of cells was routinely measured from their digital images in terms of pixels, which could be converted to real physical length based upon the diameters of silica microbeads. Figure 1 shows the schematic drawings and

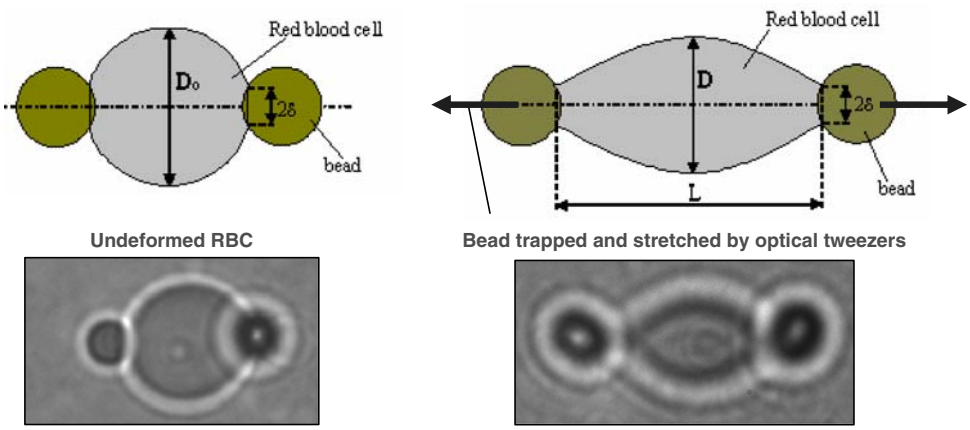

Fig. 1 Schematic drawings and microscopic images for the deformation of silica-bead-attached RBC stretched by laser tweezers

Transverse strain: $\varepsilon_t = \frac{\Delta D}{D_0} = \frac{D_0 - D}{D_0}$

Longitudinal strain: $\varepsilon_l = \frac{\Delta L}{D_0} = \frac{L - D_0}{D_0}$

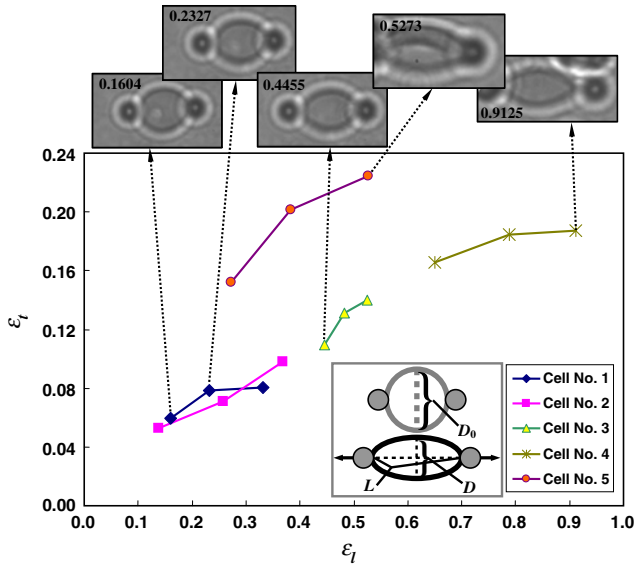

Fig. 2 Experimental measurements and selected images of deformed RBCs with attached silica microbeads (2.34 μm in diameter). The transverse and longitudinal strains are defined as $\varepsilon_t = \frac{D_0 - D}{D_0}$ and $\varepsilon_l = \frac{L - D_0}{D_0}$, respectively. The value of ε_l for each cell is shown in its photo image

microscopic photos of undeformed and stretched cells. To quantify the deformation, the transverse (ε_t) and longitudinal strain (ε_l) are introduced as following [10–12]

$$\varepsilon_t = \frac{\Delta D}{D_0} = \frac{D_0 - D}{D_0} \tag{1}$$

$$\varepsilon_l = \frac{\Delta L}{D_0} = \frac{L - D_0}{D_0} \tag{2}$$

where D_0 is the original diameter of RBCs before deformation; D and L are the maximum length perpendicular and parallel to the stretching direction. Figure 2 gives the measurements from digital images of deformed RBCs with attached silica microbeads under various stretching forces. A positive correlation between ε_t and ε_l is found, which coincide with physical intuition that larger stretching forces cause more significant lateral contraction of the cells. The numerical values of all measurements are listed in Table 1 for reader's reference.

3 Finite-element simulation

3.1 The hyperelastic solid model of cells

Hyperelasticity refers to materials that can completely recover to their original shape in a finite deformation. Many polymers and biopolymers fall into this category. The constitutive law for these materials is usually derived from a strain energy density function. The Mooney–Rivilin law is one of the best known and has been extensively used in moulding cells [13, 14].

Denoting the strain energy density function as W, the constitutive relation can be determined by the following

$$S_{ij} = \frac{\partial W}{\partial E_{ij}} = 2\frac{\partial W}{\partial C_{ij}} \tag{3}$$

where S_{ij} is the second Piola–Kirhhoff stress tensor, E_{ij} and C_{ij} are, respectively, the Lagrange and Cauchy-Green strain tensors. The second Piola–Kirhhoff stress defined in Eq. 1 is related to the Cauchy stress through the deformation gradient by

Table 1 Experimental measurements on the deformation of five RBC samples by optical tweezers

Cell No.	Diameters (pixels)	Original radius (μm)	Length of L (pixels)	Length of D (pixels)	Average 2δ (pixels)	ε_t	ε_l
1	127.606	2.96	148.082	120.003	47.539	0.0596	0.1605
			157.295	117.641		0.0786	0.2327
			169.896	117.380		0.0801	0.3314
2	138.007	3.20	156.944	130.750	53.038	0.0526	0.1372
			173.534	128.250		0.0707	0.2574
			188.858	124.500		0.0979	0.3685
3	123.548	2.87	178.594	110.013	42.636	0.1096	0.4456
			183.249	107.380		0.1309	0.4832
			188.286	106.250		0.1400	0.5240
4	125.841	2.93	207.580	105.001	47.869	0.1656	0.6495
			225.143	102.626		0.1845	0.7891
			240.670	102.251		0.1875	0.9125
5	142.743	3.31	181.598	121.000	63.255	0.1523	0.2722
			197.298	114.000		0.2014	0.3822
			218.007	110.750		0.2241	0.5273

$$\sigma_{kl} = \frac{1}{J}(f_{ki})S_{ij}(f_{jl})^{\mathrm{T}} \tag{4}$$

where the superscript T represents the transpose operations on a tensor, f_{ki} is the deformation gradient tensor and J is its determinant.

In the case of Mooney–Rivilin, a special functional form of W used in our study is

$$W = a_{10}(\bar{I}_1 - 3) + a_{01}(\bar{I}_2 - 3) + \frac{\kappa}{2}(\bar{I}_3^2 - 1)^2 \tag{5}$$

where $\bar{I}_i$ are the reduced strain invariants. Their definitions are

$$\bar{I}_1 = I_1 I_3^{-1/3}, \bar{I}_2 = I_2 I_3^{-2/3}, \bar{I}_3 = I_3^{1/2} \tag{6}$$

with the three invariants of the Cauchy-Green strain tensor: $I_1 = C_{ii}$, $I_2 = \frac{1}{2}(I_1^2 - C_{ij}C_{ij})$ and $I_3 = \det(C_{ij})$. a_{10} and a_{01} are material constants and

$$\kappa = \frac{E}{3(1-2v)} \tag{7}$$

is the bulk modulus with the relation to Poisson's ratio v and Young's modulus E. For incompressible materials, the third term in Eq. 5 vanishes because $I_3 = 1$.

3.2 Setup for finite-element analysis

The chemically swollen RBC was modelled as a sphere before deformation. As shown in Fig. 3, only quarter of the cell is needed for our analysis due to the *twofold* axisymmetry in the direction of stretch (y-axis) and along its perpendicular plane (x-axis). The commercial software ANSYS® (ANSYS 7.0, PA, USA) was employed for the analysis and its 8-node, incompressible hyperelastic element (HYPER74) was used for discretizing the computational domain. In order to simulate the experimental, the boundary conditions were setup by applying a constant stretching displacement at y-direction on the nodes near the north pole (see Fig. 3). The magnitude of stretch is according to the longitudinal strain (ε_l) based on the experimental measurements in Table 1. The resolution of mesh (total number of nodes) and step size of iteration were carefully chosen and tested to make sure that convergent results can be obtained for all cases under study.

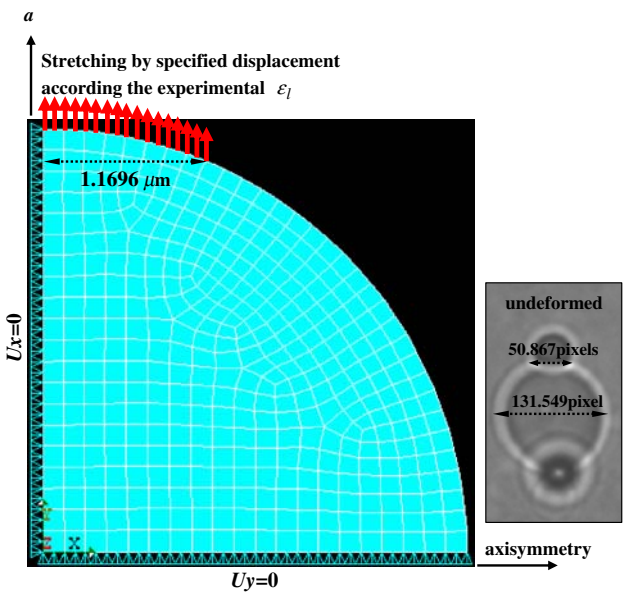

Fig. 3 The finite-element mesh and boundary conditions for numerical analysis. Radius of the chemically swollen RBC is 3.06 μm, an average value from experimental data in Table 1. A photo shows the average pixels of an undeformed RBC and the size of attached area (the ratio 50.87 pixels/131.55 pixels ≅ 1.16/3.06 μm)

3.3 Parameters for analysis

There are no demonstrative experiments in literature to provide substantial data of a_{10} and a_{01} in Mooney–Rivilin model for cells. These two constants are virtually unknown before simulations. However, both a_{10} and a_{10} represent the elastic moduli in the theory of hyperelasticity. Typical values of Young's modulus for cells range from 2×10^1 to 3×10^5 Pa, obtained by either experiments or theories from literature [15–19]. Therefore, it is well worthwhile to use this range of values for a_{10} and a_{01} in FEA initially. After extensive numerical tests, we find the values of a_{10} and a_{01} between 2×10^1 and 3×10^4 Pa are viable to obtain meaningful results. Combinations of different a_{10} and a_{01} values within that range were used in FEA again, which makes the total number of simulations more than a hundred. These simulations give us a better picture about the influence of a_{10} and a_{01} on the cell deformation.

4 Results and discussion

4.1 Cell profiles under a constant stretch

Figure 4 gives the stretched profiles of silica beads attached RBC under longitudinal strain $\varepsilon_l = 0.9125$. The values of a_{10} and a_{01} are alternatively chosen to be 1×10^3 Pa and vary the other from 1×10^2 to 30×10^3 Pa. A contour plot of the displacement field for $a_{10} = 10^3$ and $a_{01} = 10^3$ Pa are shown along side as an illustrative example. Details of local profiles near the stretch area and perpendicular plane (x-axis) are presented in Fig. 5. From the figure, we found that when $a_{10} = 10^3$, a higher a_{01} leads to less lateral contraction (smaller ε_t) of the cell. This result is physically rational since a_{10} corresponds to the stiffness for the deviatoric part of principal stretch and a_{01} the deviatoric part of area change, following the

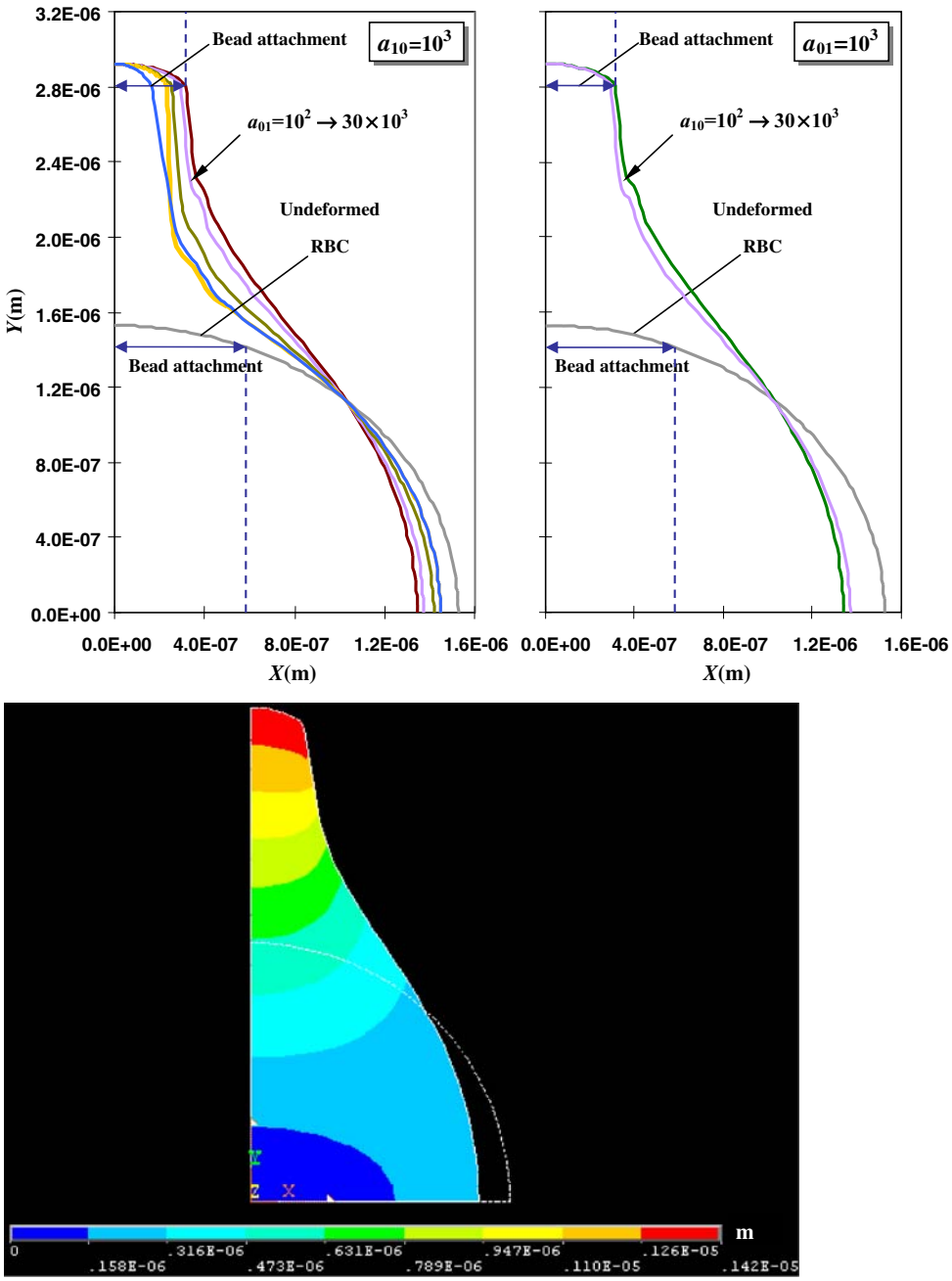

Fig. 4 Deformation profiles of FEA-simulated RBC for cases of $\varepsilon_l = 0.9125$ (cell no. 4) under different Mooney–Rivilin constants. An example of the numerical results for $a_{10} = 10^3$ and $a_{01} = 10^3$ Pa is presented in the contour plot of displacement field. Details of local profiles are shown in Fig. 5. The scales of X/Y-axis are 50% reduction (half) of the real scales

expression in Eq. 5. Higher a_{01} implies more resistance to the area change. This reasoning vice versa explains the cases of $a_{01} = 10^3$ in which a higher a_{10} causes more lateral contraction. Figure 5 also implicitly indicates that for a fixed value of a_{01}, the lateral contract is less sensitive to the variations of a_{10}.

4.2 Comparisons between experiment and simulation

To determine the appropriate range of Mooney–Rivilin constants for RBCs, a comparison based on the minimization of discrepancy between experimental and numerical results among different a_{10} and a_{01} values were carried out based on the following criteria:

$$\min \sqrt{\sum_{\substack{\text{experimental} \\ \text{datapoint}}} \left(\varepsilon_t^{\exp} - \varepsilon_t^{\text{num}}\right)^2} \tag{8}$$

Figure 6 shows the respect average errors for cases of $a_{10} = 10^3$ and $a_{01} = 10^3$ Pa. As it can be seen that when $a_{10} = 10^3$ Pa, the errors approach a constant if a_{01} is high enough (>5,000 Pa most likely). Similarly, when $a_{01} = 10^3$, higher a_{10} brings the numerical results closer to

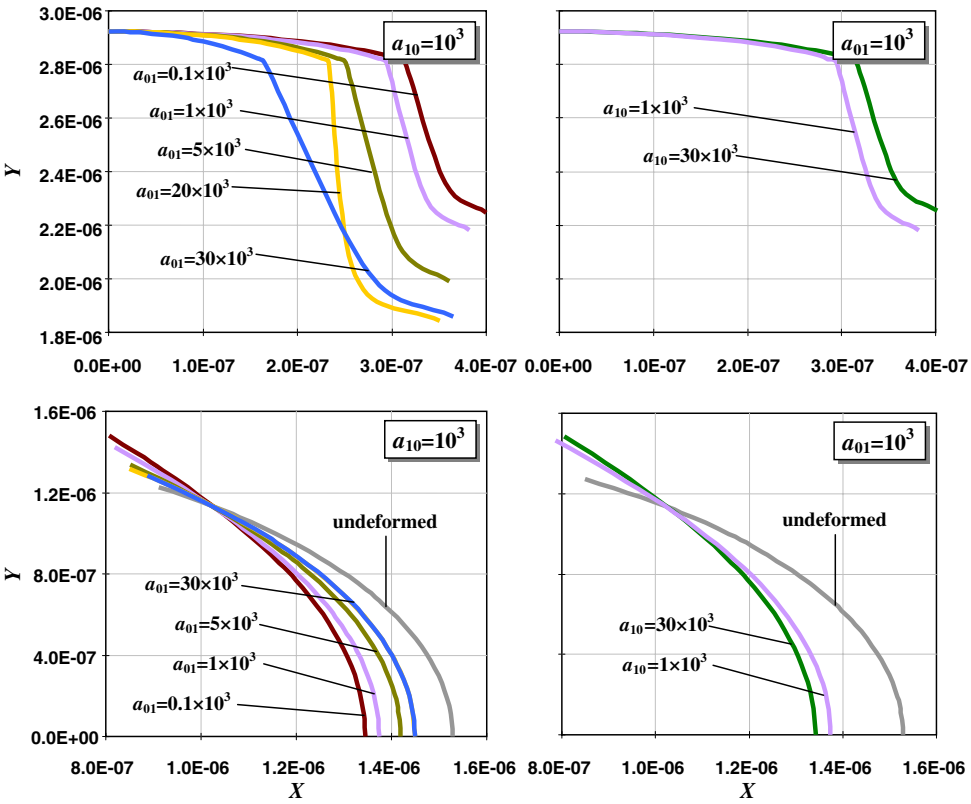

Fig. 5 Local profiles of deformed RBC from FEA for cases of $\varepsilon_l = 0.9125$ under different Mooney–Rivilin constants. The scales of X/Y-axis are 50% reduction (half) of the real scales

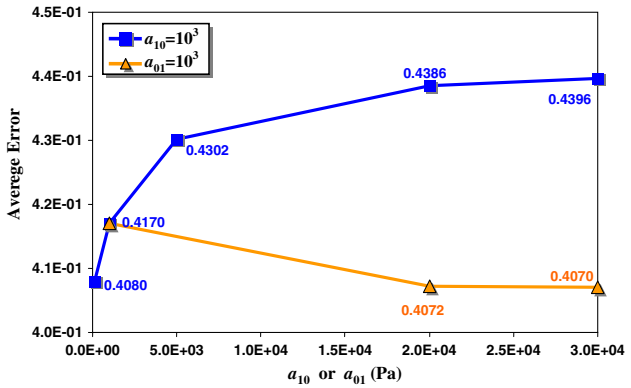

Fig. 6 Average errors in the transverse strain ε_t between the experimental data and FEA results

the experiment. However, the variations of a_{10} has less influence on the later contraction of cells.

5 Conclusions

Optical tweezers have been demonstrated as a powerful tool to characterize the deformation and mechanical properties of biological cells. In combination with an appropriate material model and FEA, the experimental measurement of cell deformations under optical trapping can facilitate the determination of material properties of cells in a quantitative manner. The FEA-based simulation has been carried out to determine the two critical constants proposed in the Mooney–Rivlin material law. By a parameter study to minimizing the discrepancy between experimental and numerical data in the transverse strain, values of the two constants between 2×10^1 and 3×10^4 Pa have been found to have the optimal results. The combination of laser tweezers and FEA-simulations provides an affable and economical means to study the deformation and mechanical properties of the cells as compared with other techniques such as micropipette aspiration and atomic force microscope indentation [20].

Acknowledgement KKL would like to thank the financial support from BBSRC/EPSRC (BB/D014786/1).

References

1. D.E. Discher, N. Mohandas, E.A. Evans, Science **266**(5187), 1032 (1994)
2. F.K. Glenister, R.L. Copper, A.F. Cowman, N. Mohands, B.M. Cooke, Blood **99**(3), 1060 (2002)
3. L.H. Miller, D. I. Baruch, K. Marsh, O.K. Doumbo, Nature **415**(6872), 673 (2002)
4. L. Rossi, S. Serafini, F. Pierigé, A. Antonelli, A. Cerasi, A. Fraternale, L. Chiarantini, M. Magnani, Expert Opin. Drug Deliv. **2**(2), 311 (2005)
5. S. Hénon, G. Lenormand, A. Richert, F. Gallet, Biophys. J. **76**, 1145 (1991)

6. D.A. Grier, Nature **424**, 810 (2003)
7. J.A. Sleep, D., Wilson, R.M. Simmons, W.B. Gratzer, Biophys. J. **77**, 3085 (1999)
8. K. Svoboda, S.M. Block, Ann. Rev. Biophys. Biomol. Struct. **23**, 247 (1994)
9. K. Köig, Histochem. Cell Biol. **114**, 79 (2000)
10. J. Guck, R. Ananthakrishnan, H. Mahmood, T.J. Moon, C.C. Cunningham, J. Kas, Biophys. J. **81**, 767 (2001)
11. K.H. Parker, C.P. Winlove, Biophys. J. **77**, 3096 (1999)
12. J.J. Foo, K.K. Liu, V. Chan, AIChE J. **50**(1), 249 (2004)
13. R. Skalak, Biorheology **10**, 229 (1973)
14. D. Barthes-Biesel , A. Diaz, E. Dhenin, J. Fluid Mech. **460**, 211 (2002)
15. G.K. Ragsdale, J. Phelps, K. Luby-Phelps, Biophys. J. **73**, 2798 (1997)
16. C. Rotsch, K. Jacobson, M. Radmacher, Proc. Natl. Acad. Sci. **96**, 921 (1999)
17. U.G. Hofmann, C. Rotch, W.J. Parak, M. Radmacher, J. Struct. Biol. **110**, 84 (1997)
18. L.J. Gibson, M.F. Ashby, Proc. R. Soc. Lond. A **382**, 43 (1982)
19. C. Li, Y.P. Liu, K.K. Liu, J.H. Hsieh, Comp. Mater. Sci. **30**, 504 (2004)
20. D. Boal, *Mechanics of the Cell* (Cambridge University Press, Cambridge, UK, 2002)